An Experimental Laser Guide Star Wavefront Sensor Simulator

Olivier Lardière, Rodolphe Conan, Colin Bradley, and Kate Jackson

AO Laboratory, Mechanical Engineering Department, University of Victoria, PO Box 3055 STN CSC, Victoria, BC, V8W 3P6, Canada

Glen Herriot

NRC–Herzberg Institute of Astrophysics, 5071 W. Saanich Rd, Victoria, BC, V9E 2E7, Canada

ABSTRACT

Sodium laser guide stars (LGSs) allow, in theory, full sky coverage, but have their own limitations. Variations of sodium layer altitude, thickness and atom density profile induce changing errors on wavefront measurements (LGS aberrations), especially with ELTs for which the LGS spot elongation is larger. In the framework of the Thirty–Meter–Telescope project (TMT), the AO–Lab of the University of Victoria (UVic) built a LGS–simulator test bed in order to assess the performance of new centroiding algorithms for LGS Shack-Hartmann wavefront sensors (SH–WFS). The principle of the LGS–bench is briefly reviewed. The closed–loop performances of the matched filter (MF) algorithm on laboratory 29×29 elongated spot images are presented and compared with the centre of gravity (CoG). The ability of the MF to track the LGS aberrations is successfully demonstrated. The UVic LGS–bench is not limited to SH–WFS and can serve as a LGS–simulator test bed to any other LGS–AO projects for which sodium layer fluctuations are an issue.

Keywords: Adaptive Optics, Laser guide star, Wavefront sensing

1. INTRODUCTION

Laser guide star (LGS) adaptive optics (AO) systems allow, in theory, full sky coverage, but have their own limitations, such as the tilt indetermination[1] and the cone effect.[2] With Extremely Large Telescopes (ELTs), other difficulties appear when using a sodium LGS for two main reasons. Firstly, the artificial star is not a point–like source but an extended source along the laser beam axis due to the sodium layer thickness. Secondly, the sodium layer is not static but ever–changing. The mean altitude fluctuates, as well as the thickness and the sodium atom density vertical profile, with a time–scale of about one minute or less.[3] This temporal variability induces changing errors in wavefront measurements, especially with ELTs, for which the source elongation is larger.

Fluctuations of sodium layer mean altitude induce a focus error which can be almost cancelled by closed–loop focus tracking using a Natural Guide Star (NGS) wavefront sensor (WFS), zoom optics and electronic offsets. A zoom optics focus loop is already implemented on the Keck LGS–AO system,[4] and optical focusing plus electronic offsets are planned for NFIRAOS,[5] the LGS–AO facility of the Thirty–Meter–Telescope (TMT). Despite that correction, a residual focus and higher mode error, referred to as LGS aberrations,[6,7] remains and affects the closed–loop performance of AO systems. New centroiding algorithms are under study to mitigate LGS aberrations with SH–WFSs, such as the matched filter[8] (MF) or the correlation.[9,10] Radial CCD arrays are also under development[11] to reduce the number of required pixels and mitigate also square–symmetric LGS aberrations.

In the framework of the TMT project, the AO–Laboratory of the University of Victoria (UVic) has built an LGS–simulator bench[7] in order to assess the performance of wavefront sensing algorithms when using sodium LGS SH–WFS, in particular the MF centroiding algorithm planned for NFIRAOS.

This paper reviews the goal and the basic principle of the Uvic LGS–bench simulator (Sec. 2) and of the MF algorithm implemented on the bench (Sec. 3). The dynamical performances of the MF in open loop are compared to those obtained with the Centre of Gravity (CoG) algorithm on variable sodium profiles (Sec. 4).

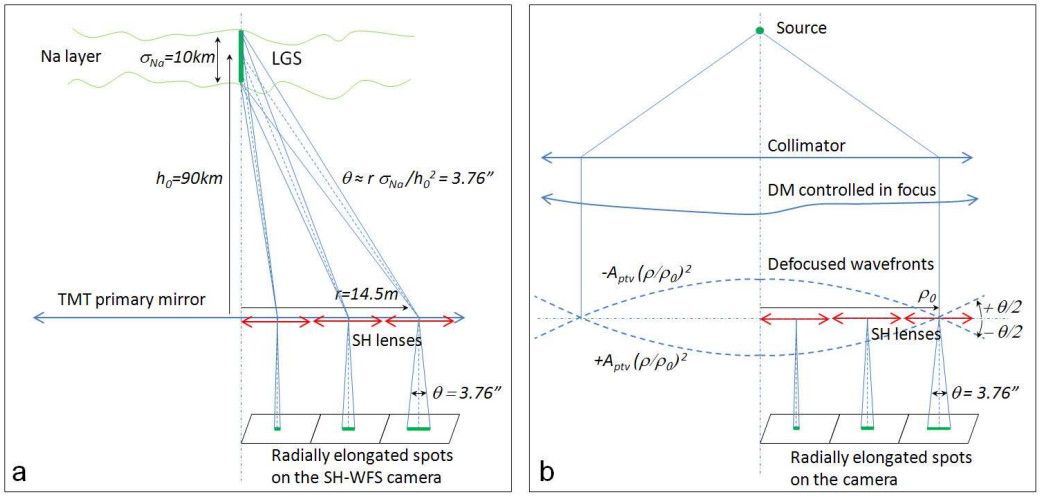

Figure 1. (a) SH–WFS spots geometry for the TMT pupil pointing a LGS at zenith. (b) The radial elongation of the spots can be reproduced in the laboratory with a DM generating an alternating defocus during the integration time of the SH–WFS camera. The source intensity is modulated synchronously with the DM to also reproduce sodium profile variations.

Section 5 presents the performance for different signal–to–noise ratios (SNR). Lastly, some turbulence is added in closed–loop to check the ability of the MF to correct the wavefront of the turbulence, regardless of sodium layer variations (Sec. 6).

2. DESCRIPTION OF THE LGS–BENCH

As the TMT laser launch telescope will be located behind the secondary mirror, a LGS SH–WFS image will feature radially elongated spots from the pupil centre (Fig. 1a). The UVic LGS–bench reproduces in laboratory the following features:

- the spot radial elongation due to the sodium layer thickness, with 2×8 pixels for the most elongated spots,
- the spatial and temporal variability of the sodium layer (mean altitude, thickness and vertical profile),
- the focus tracking loop planned in the NFIRAOS design to follow the sodium layer mean altitude variation,
- the dithering tip/tilt signal required by the matched filter algorithm,
- the residual atmospheric turbulence.

The basic principle of the LGS–bench is sketched on Fig. 1b. The LGS–bench is fully described in Ref. 7. The LGS test bed is based on a simple design using only a few components namely a laser diode, a 8×8 actuator DM and a 29×29 lenslet SH–WFS. The bench reproduces with a great accuracy 29×29 LGS elongated in the same conditions than the TMT (Fig. 2). The bench is entirely controlled within the Simulink environment allowing the rapid prototyping of algorithm which are first developed and tested by simulation before to be ported to the bench. The data containing the sodium profiles come from a time series of 88 real profiles measured by the Purple Crow LIDAR (University of Western Ontario) and used inside the TMT consortium as a benchmark (Fig. 3).

3. PRINCIPLE OF THE MATCHED FILTER

Basically, a local wavefront slope θ shifts the spot of the corresponding subaperture image I. For small slopes:

$$I(\theta) - I(0) = G\,\theta + noise\,, \tag{1}$$

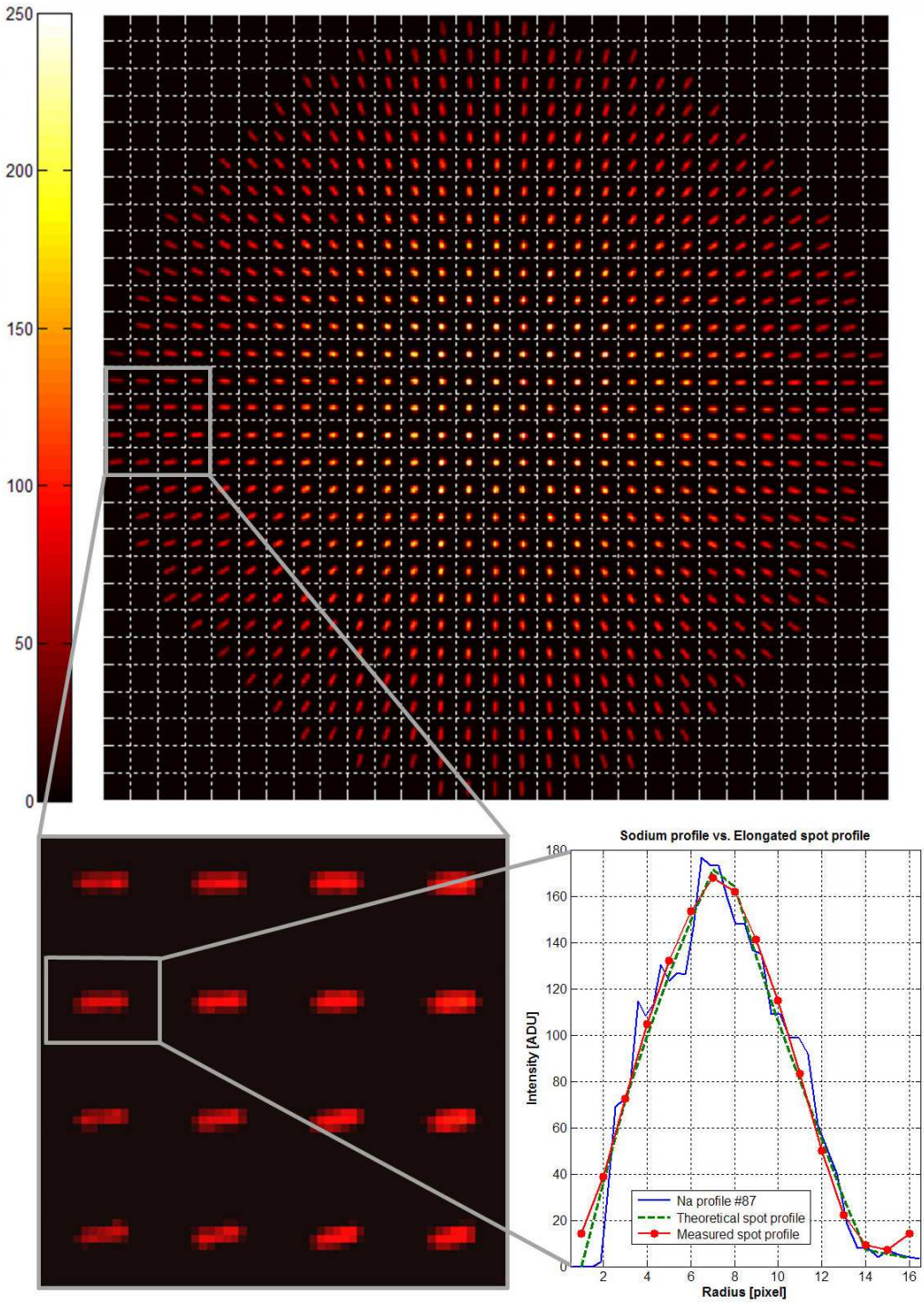

Figure 2. 29×29 elongated spot SH–WFS image obtained in laboratory. Spot sampling is 2×8 pixels on the edge of the pupil (for a 10 km–thick sodium profile) as for NFIRAOS (see enlarged spots). The sodium profile used for this image is the 87^{th} profile of the LIDAR sequence (Fig. 3). The solid curve shows the intensity profile sent to the source (*i*.e. the projected sodium profile sampled over 41 altitude bins). The dashed curve shows the theoretical profile for a spot located on the edge of the pupil (*i*.e. the source intensity profile convolved by the PSF and re-sampled over 16 pixels). The measured spot profile (filled circles) perfectly matches the theoretical spot profile, except for the pixel 16 where the spot overlaps with another.

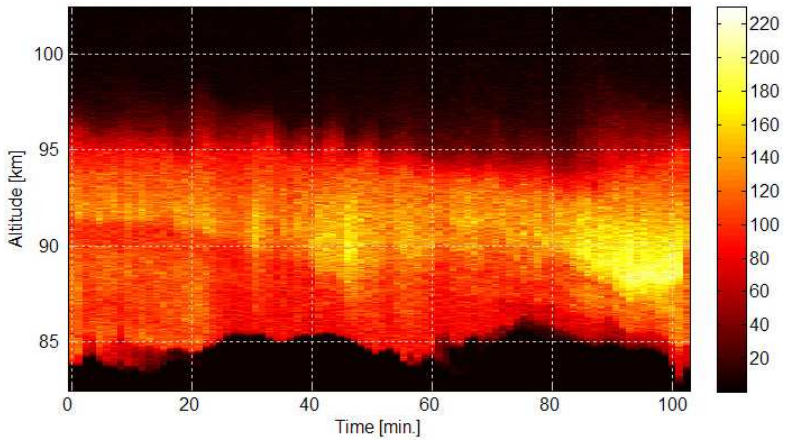

Figure 3. Sequence of 88 real sodium profiles used for generating LGS–like SH–WFS images on the bench. Data from Purple Crow LIDAR (Univ. of Western Ontario). Time resolution is 70 s, altitude resolution is 25 m (file TMT.AOS.TEC.07.005).

with $I(\theta)$ and $I(0)$ the intensity distribution of the shifted image and of the reference image respectively. G is the intensity pixel gain estimated on the bench by dithering and synchronous detection[12] (mathematically $G = dI/d\theta$). Equation 1 can be written for whole subaperture slopes and images using a matrix notation:

$$\theta = \mathbf{R}\,(\mathbf{I} - \mathbf{I_0})\,, \tag{2}$$

with $\mathbf{R}$ the Matched Filter matrix, *i*.e. the noise–weighted pseudo–inverse of $\mathbf{G}$. The reference image $\mathbf{I_0}$ and the gain $\mathbf{G}$ are periodically updated in order to track the sodium layer variations. The MF is constrained to improve its dynamic–range. The full theory of the MF algorithm is presented in Ref. 8.

The MF algorithm was developed and tested apart with Simulink on simulated images before its implementation on the LGS–bench.[12] A tip/tilt dithering signal is generated by the DM. A tip/tilt closed–loop tracks the bench drifts, while a focus closed–loop tracks the mean altitude change of the sodium layer. Lastly, an AO closed–loop corrects the higher modes. The content of the MF block is detailed in Ref. 12 of these proceedings.

4. PERFORMANCE WITH VARIABLE SODIUM PROFILES AND HIGH SNR

4.1 WAVEFRONT ANALYSIS PROCEDURE

Wavefront analysis were now made with a time series of 88 sodium profiles (Fig. 3) to check the ability of the updated MF to mitigate the LGS aberrations. The time resolution of the sodium profile sequence is 70 s. As there are no turbulence in this analysis, the sodium profile sequence can be played in fast motion. The MF is updated 8 times per profiles, this update rate giving the best results (Sec. 4.3). The sodium profiles are interpolated in order to generate continuous variations.

The dithering amplitude is 0.01 pixel for the following measurements. Temporal mean values and standard deviations of slope measurements are calculated from the sequence, as well as the reconstructed phase in term of Zernike modes.

Moreover, we suggest to compare the results of the MF to the conventional CoG, but also to a dynamically referenced CoG, refereed to as DRCoG. This comparison is more fair and allows us to distinguish the specific advantages of the MF. Actually, the MF is assumed to give better performances for 2 distinct reasons:

- (i) the use of pixel intensity gain to compute slopes,
- (ii) the use of updated references to follow the sodium layer changes.

In a very similar way, the CoG algorithm can also use the reference image I_o (already used by the MF) to update the centroid offsets and track the sodium variations. The centroids of the last image I can be computed as follow:

$$\text{slopes} = CoG(I) - CoG(I_o). \tag{3}$$

Table 1. Typical wavefront *ptv* errors measured on the bench by the CoG, DRCoG and MF, during the 88 Na profile time series, without turbulence and SNR=140 for central spots. The DRCoG and the MF are updated 8 times per Na profile. ϕ is the total mean phase error in nm *ptv* (*i*.e. static aberrations). σ_ϕ is the total temporal RMS fluctuations (in nm *ptv rms*) of the wavefront (tip/tilt and focus modes are removed), while σ_{Z11}, σ_{Z14} and σ_{Z22} are the RMS fluctuations for the three detectable LGS aberrations.[6]

	CoG	DRCoG	MF
ϕ	120	5.93	0.10
σ_ϕ	25.5	7.03	3.52
σ_{Z11}	25.5	7.03	2.40
σ_{Z14}	7.80	2.51	1.78
σ_{Z22}	3.13	1.81	0.60

4.2 RESIDUAL LGS ABERRATIONS

Figure 4 presents the wavefront measurements of the MF compared to the conventional CoG and to the DRCoG. As foreseen, the static aberrations (due to misalignment errors), seen by the CoG, disappear with the DRCoG and the MF (because both are relative WFSs).

The temporal RMS errors due to the LGS fluctuations, such as Z_{11} and Z_{14}, are partially cancelled by the DRCoG, and totally cancelled by the MF. Actually, the RMS error measured for Z_{11} is 25 nm *ptv rms* for the CoG, 7 nm *ptv rms* for the DRCoG, and only 2.5 nm *ptv rms*, *i*.e. the bench accuracy, for the MF (Tab. 1).

These first laboratory results prove the intrinsic superiority of the MF for LGS WFS over the CoG, even dynamically referenced.

4.3 PERFORMANCE VERSUS THE UPDATE RATE

Previous results are obtained for a MF updated 8 times per sodium profiles. Figure 5 displays now the RMS error for Z_{11}, the dominant LGS aberration, for different update rates, without turbulence.

If the MF is updated just once at the start of the sodium profile sequence (first point of the plot), the RMS error reaches 9 nm *ptv rms*, 2.7 times smaller than the error measured by the CoG (25 nm). This error is reduced to the ultimate accuracy of the bench (about 2.4 nm *ptv rms*) if the MF is updated at least 8 times per sodium profile.

Similarly, if the update rate of the DRCoG is low, the error is roughly close to the error measured by the CoG, as foreseen. Best results are obtained if the DRCoG is referenced at least 8 times per sodium profile too. But whatever the update rate, the DRCoG error remains 3 to 4 times greater than the MF error.

The MF performance remains superior whatever the update rate. Eight updates per profiles seems optimal with the sodium layer sequence we are using, *i*.e. an actual update period of about 9 s on the sky, which lets enough time to average the turbulence.

5. PERFORMANCE AT LOW FLUX

The performance of the MF is now compared to the CoG for various SNR. The source intensity is dimmed to decrease the SNR. For each SNR, the MF is computed with and without the covariance noise matrix C_η.[8] A "radial" threshold is applied on the CoG algorithm to improve its performance at low flux. Best results are obtained if the threshold is equal to 8% of the maximum of the local sub-image.

Figure 6 plots the RMS slope error of the CoG and MF for SNR from 10 to 170. The MF gives better performances for SNR lower than 50. At SNR=18 (expected SNR for TMT), the MF gives the same accuracy than a radially thresholded CoG (resp. unthresholded CoG) using a laser power 1.8 (resp. 2.5) times greater.

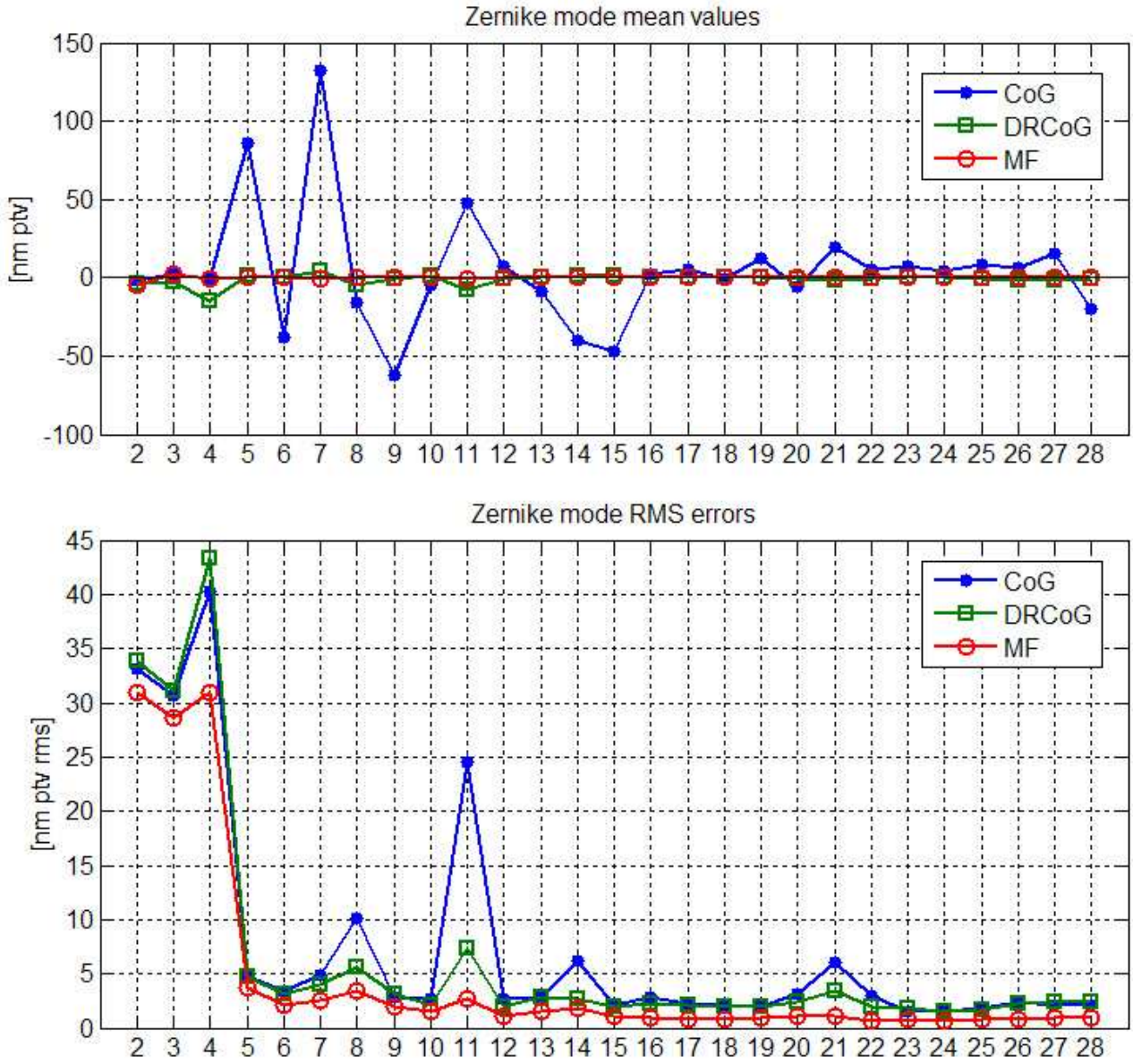

Figure 4. Static aberrations and temporal RMS errors for the 28 first Zernike modes measured during the sodium profile sequence for the CoG, the DRCoG and the MF. The 35 nm *ptv* tip/tilt RMS error is due to the dither signal, which is not removed, and to the residual jitter of the bench. The 40 nm *ptv* focus RMS error is due to the spot elongation and to the residual error of the bench focus loop. The fluctuation in coma (Z_8) is not a LGS aberration, but it is due to calibrations errors of the DM. The unexpected Z_{21} (pentafoil) fluctuation is likely due to bench misalignment errors or DM miscalibration errors; the neighbouring LGS–induced Z_{22} mode could also stimulate some Z_{21}. DRCoG and MF are updated 8 times per Na profile (1 Na profile lasts 70s on the sky, and profiles are interpolated). CoG and DRCoG threshold = 13 ADU for whole lenslets. SNR=140 for central spots.

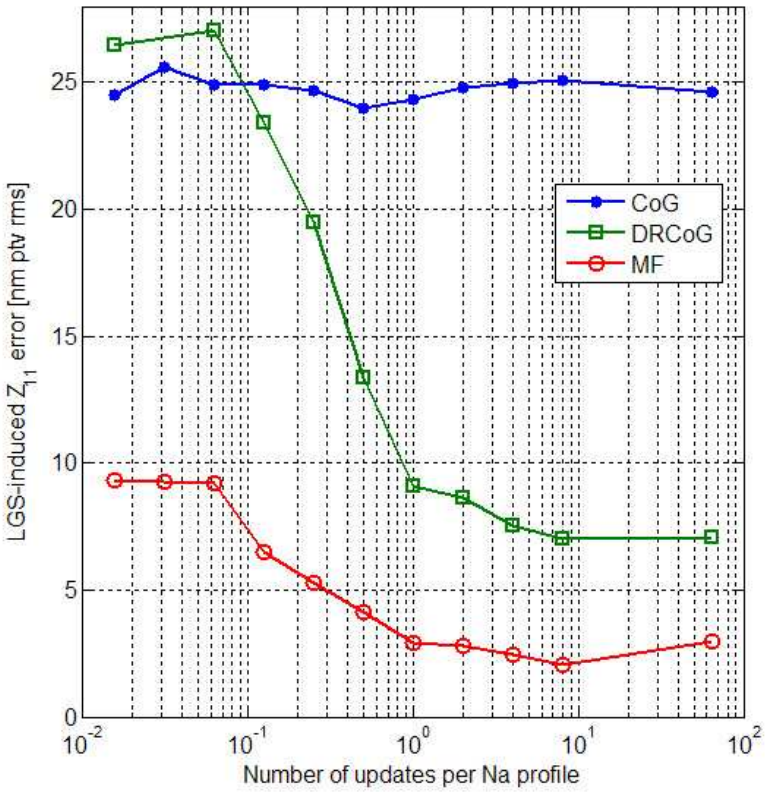

Figure 5. LGS–induced Z_{11} error versus the update rate of MF and DRCoG. CoG and DRCoG threshold = 13 ADU for whole lenslets. SNR=140 for central spots.

6. PERFORMANCE IN CLOSED–LOOP WITH TURBULENCE AND VARIABLE SODIUM PROFILES

Some low spatial frequency turbulence can be added thanks to the 8×8 actuator DM of the bench. A Kolmogorov turbulent phase screen time series is generated off–line by the computer and converted into a voltage array. These voltage offsets are electronically added to the DM voltages to generate the desired phase screens. Piston, tip, tilt and focus modes are removed from the turbulence phase screens to not interact with the separate tip/tilt and focus loops. Modes higher than Z_{30} are also removed to obtain a better correction with the 8×8 actuator DM, and minimize the contribution of the DM fitting error.

A typical phase screen snapshot is visible on Fig. 7. The input turbulence features a WFE around 555 nm *rms* (3μm *ptv*), while the residual closed–loop WFE is about 28 nm *rms* (200nm *ptv*). The AO correction is limited by the DM, not by the MF (or CoG) WFS noise.

When the MF closes the AO loop, only the turbulence should be corrected, not the LGS aberrations seen by the CoG. As described previously in Sec. 4, the LGS aberration reach 25nm and are dominated by Z_{11}. In order to be able to detect such small aberrations among the residual turbulence, the measurements were performed with SNR=140, instead of $SNR = 18$, to improve the AO correction.

The timescale ratio between the turbulence and the sodium layer reaches 10^4 typically, requiring a huge number of iterations to simulate a LGS during several minutes (on the sky) with the bench (the bench provides only 4 images per seconde, centroid computation included). Thus, to accelerate and exaggerate the LGS variations, four extreme sodium profiles has been selected from the whole sodium sequence and reproduced successively with a 4 s time scale only instead of 70 s (the profiles are still interpolated to generate a continuous variation). This case is pessimistic for the MF, but allow us to perform the experiment in the lab in a reasonable short time (less than 1 hour).

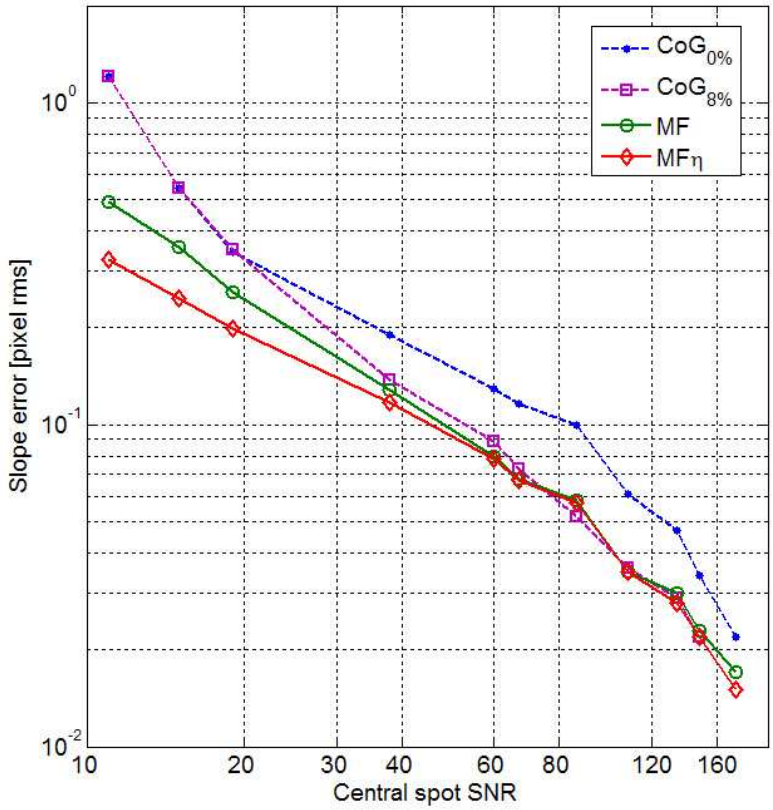

Figure 6. Mean slope error (averaged over the pupil) for different SNR on a static Na profile. $CoG_{x\%}$ denotes a CoG algorithm using images thresholded at $x\%$ of the sub–image maximum. $MF\eta$ is the matched filtering computed with the noise covariance matrix C_η.

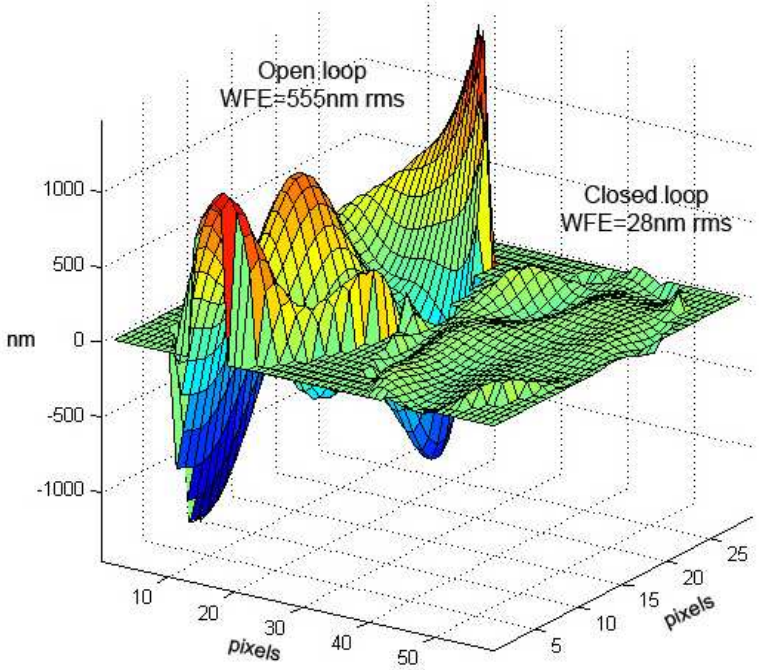

Figure 7. Typical snapshot wavefronts of the input turbulence (open–loop) and of the residual turbulence after correction (closed–loop).

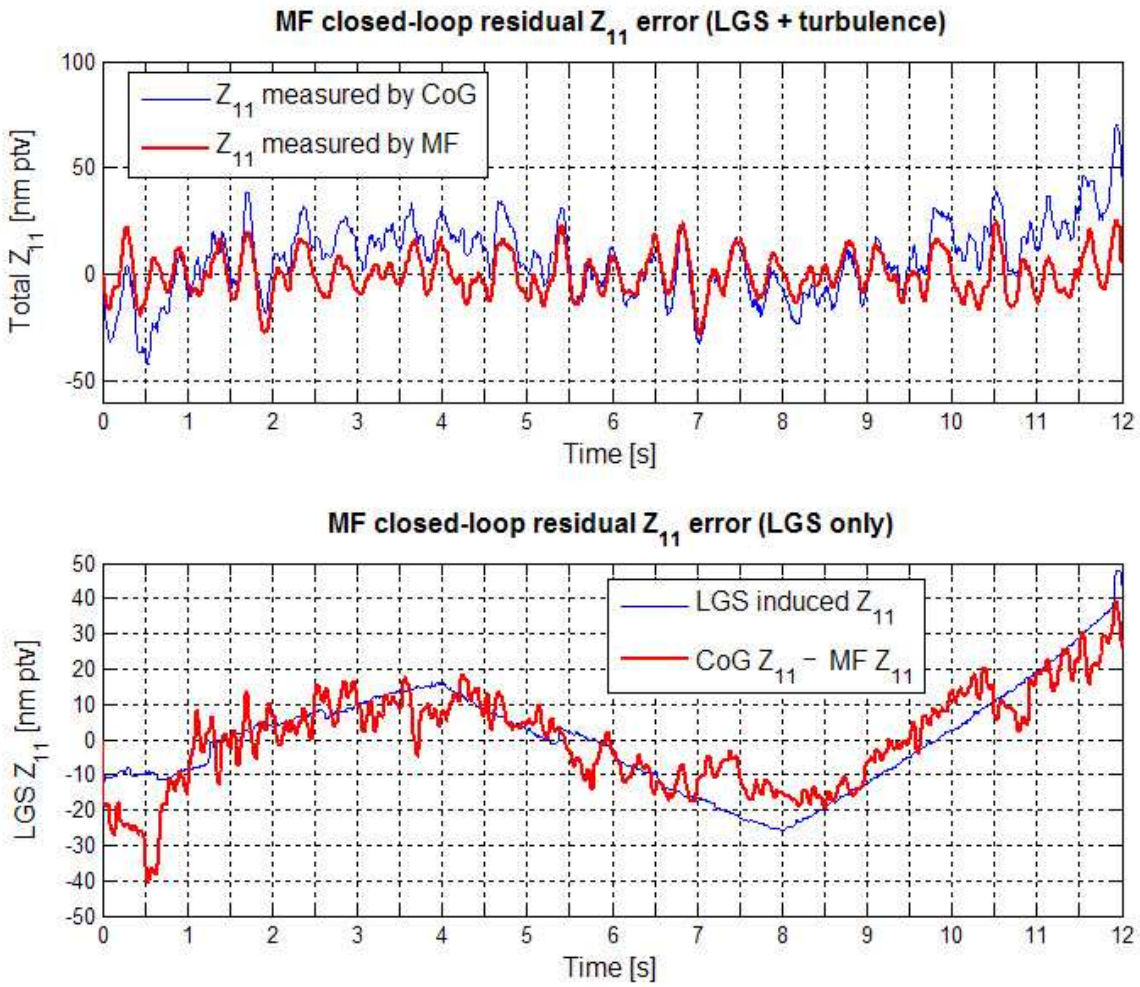

Figure 8. Residual error when the MF closes the AO loop with some turbulence and Na layer fluctuations. Top: Temporal variation of the residual Z_{11} (due to LGS plus residual turbulence) seen by the CoG and the MF. Bottom: expected LGS induced Z_{11} (measured without turbulence in open loop by the CoG) compared to the measured residual LGS induced Z_{11} (given by the difference of the CoG and the MF). Sodium layer variations are accelerated 17.5×, the MF update period is 0.5s, SNR=140.

Figure 8 displays the temporal variation of Z_{11} versus the time, seen by the CoG and by the MF. The CoG should measure both the LGS and the residual turbulence aberrations, while the MF is supposed to detect only the residual turbulence. Thus, the difference of the CoG and the MF should contain only the LGS aberrations, which is the case, except during the 2 fist update periods (*i*.e. 1 s here) needed to properly initialize the MF. The LGS aberration tracking error is only about 6.8nm *rms* after the 2^{nd} update for this worse case. This good result has to be compared to the intrinsic accuracy of the bench for Z_{11} (in open–loop without turbulence) which is 2.5nm *rms* (Tab. 1).

7. CONCLUSION

The UVic AO–Lab has built a LGS–simulator bench for the TMT project in order to assess the performance of wavefront sensing when using sodium LGSs. The bench reproduces with a great accuracy 29×29 LGS elongated in the same conditions than the TMT, with turbulence and sodium layer variability.

The Matched Filtering algorithm has been implemented and tested on the bench, in open and closed–loop, with turbulence and variable sodium profiles. The MF is intrinsically more accurate than CoG (30–40%) to

estimate the slopes, moreover, the MF mitigates the LGS aberrations from 25nm to 3.5nm rms (instead of 7.5nm with a Dynamically Referenced CoG).

The MF exhibits very good performance at low SNR, relaxing the laser power constrain by a factor 1.8 compared to the CoG. Lastly, in closed–loop the MF corrects only the turbulence and lets the LGS aberrations almost unchanged. The LGS aberration tracking error is 6.8nm *rms* in a worse case scenario.

These results are a successful demonstration in laboratory of the LGS aberration tracking by the MF in presence of turbulence. The next step is the implementation on the LGS–bench of the Truth WFS planned for NIFRAOS, as well as the algorithm blending data coming from the Truth WFS with those coming from the LGS WFS.

ACKNOWLEDGMENTS

Authors are grateful to TMT consortium. The TMT Project gratefully acknowledges the support of the TMT partner institutions. They are the Association of Canadian Universities for Research in Astronomy (ACURA), the California Institute of Technology and the University of California. This work was supported as well by the Gordon and Betty Moore Foundation, the Canada Foundation for Innovation, the Ontario Ministry of Research and Innovation, the National Research Council of Canada, the Natural Sciences and Engineering Research Council of Canada, the British Columbia Knowledge Development Fund, the Association of Universities for Research in Astronomy (AURA) and the U.S. National Science Foundation.

REFERENCES

[1] F. Rigaut and E. Gendron, "Laser guide star in adaptive optics : The tilt determination problem," Astron. Astrophys. **261,** 677–684 (1992).

[2] M. Talon and R. Foy, "Adaptive telescope with laser probe : Isoplanatism and cone effect," Astron. Astrophys., **235,** 549–557 (1990).

[3] D. S. Davis, P. Hickson, G. Herriot, and C-Y She, "Temporal variability of the telluric sodium layer," Opt. Lett. **31,** 3369–3371 (2006).

[4] M. A. van Dam, A. H. Bouchez, D. Le Mignant, E. M. Johansson, P. L. Wizinowich, R. D. Campbell, J. C. Chin, S. K. Hartman, R. E. Lafon, P. Jr. Stomski, and D. M. Summers, "The W. M. Keck Observatory Laser Guide Star Adaptive Optics System: Performance Characterization", Publi. of the Astron. Soc. of the Pacific **118,** 310-318 (2006).

[5] G. Herriot, P. Hickson, B. L. Ellerboek, D. A. Andersen, T. Davidge, D. A. Erickson, I. P. Powell, R. Clare, L. Gilles, C. Boyer, M. Smith, L. Saddlemyer, J.-P. Véran, "NFIRAOS: TMT narrow field near-infrared facility adaptive optics," in *A*dvances in Adaptive Optics II, B. Ellerbroek, D. Bonaccini Calia, eds., Proc. SPIE **6272,** (2006).

[6] R. M. Clare, M. A. van Dam and A. H. Bouchez, "Modeling low order aberrations in laser guide star adaptive optics systems," Opt. Express **15,** 4711–4725 (2007).

[7] O. Lardière, R. Conan, C. Bradley, K. Jackson and G. Herriot,"A laser guide star wavefront sensor bench demonstrator for TMT,", Opt. Express **16,** 5527–5543 (2008).

[8] L. Gilles and B. Ellerbroek, "Constrained Matched Filtering for Extended Dynamic Range and Improved Noise Rejection for Shack-Hartmann Wavefront Sensing," Opt. Lett. **33,** 1159-1161 (2008).

[9] L. A. Poyneer, "Scene-based Shack-Hartmann wave-front sensing: analysis and simulation," Appl. Opt. **42,** 5807–5815 (2003).

[10] S. Thomas, T. Fusco, A. Tokovinin, M. Nicolle, V. Michau and G. Rousset, "Comparison of centroid computation algorithms in a ShackHartmann sensor," Mon. Not. R. Astron. Soc. **371,** 323-336 (2006).

[11] J. W. Beletic, S. Adkins, B. Burke, R. Reich, B. Kosicki, V. Suntharalingham, Ch. Bleau, R. Duvarney, R. Stover, J. Nelson and F. Rigaut, "The Ultimate CCD for Laser Guide Star Wavefront Sensing on Extremely Large Telescopes," Experimental Astronomy **19,** 103–109 (2005).

[12] R. Conan,"NFIRAOS Laser Guide Star Wavefront Sensing Control algorithms," Proc. SPIE **7015,** in press (2008).